Materials Today Communications 11 (2017) 163–173

Contents lists available at ScienceDirect

Materials Today Communications

journal homepage: www.elsevier.com/locate/mtcomm

Nucleation effect of unmodified graphene nanoplatelets on PVDF/GNP film composites

Hossein Cheraghi Bidsorkhi[a,b,*], Alessandro Giuseppe D'Aloia[a,b,*], Giovanni De Bellis[a,b], Alessandro Proietti[a,b], Andrea Rinaldi[a,b], Marco Fortunato[a,b], Paolo Ballirano[b,c], Maria Paola Bracciale[b,d], Maria Laura Santarelli[b,d], Maria Sabrina Sarto[a,b]

[a] Dept. of Astronautical, Electrical and Energy Engineering, Sapienza University of Rome, via Eudossiana 18, 00184 Rome, Italy
[b] Research Center on Nanotechnology Applied to Engineering of Sapienza (CNIS), Sapienza University of Rome, via Eudossiana 18, P.le Aldo Moro 5, 00185 Rome, Italy
[c] Dept. of Earth Sciences, Sapienza University of Rome, P.le Aldo Moro 5, 00185 Rome, Italy
[d] Dept. of Chemical Engineering Materials and Environment, Sapienza University of Rome, via Eudossiana 18, 00184 Rome, Italy

ARTICLE INFO

Keywords:
Film composite
PVDF
Graphene nanoplatelets
β-Phase
Phase transformation
Porosity
Chain orientation
Nucleation effect
Electromechanical properties

ABSTRACT

Development of polyvinylidene fluoride (PVDF) film composite filled with carbon-based nanomaterials is attracting considerable attention in engineering applications. Numerous studies focus on the enhancement of PVDF properties by adding chemically modified graphene oxide or functionalized carbon nanotubes, or by modifying the polymer chains. On the other hand, in this paper we investigate the nucleation effect of graphene nanoplatelets (GNPs) on morphology and structure of PVDF, without any chemical modification or functionalization either of the GNPs or of the polymer chains. Thus, we fabricate GNP-filled PVDF composite films by the solution casting method. Then, we investigate the effect of GNPs on composite porosity, crystallinity and polymer phases, with special emphasis on the formation of β-phase. To this purpose, the produced PVDF/GNP composite films are characterized through scanning electron microscopy and atomic force microscopy topographies, differential scanning calorimetry, X-ray powder diffraction and Fourier transform infrared spectroscopy. All these experimental characterizations show that GNPs uniformly dispersed in PVDF, without any modification or functionalization, influence significantly the polymer structure and porosity, enhancing the β-phase crystals formation. Finally, the electrical, mechanical and electromechanical properties of the produced PVDF/GNP composite films are characterized.

1. Introduction

In the past two decades, polymer-based nanocomposite have attracted considerable academic and industrial attention [1,2]. In fact, the rapid development of electronic devices has led to a large demand for polymeric materials with good electrical conductivity and thermal stability, as well as mechanical strength [3–5]. Nowadays, conventional polymeric materials usually exhibit low modulus and poor electrical conductivity, thus requiring the addition of conducting fillers to improve their electrical, mechanical and physical properties. Nevertheless, high filler loadings generally lead to low mechanical strength and ductility, as well as poor processability of polymer nanocomposite. In this context, nanometric sized fillers have gained a crucial role. The most studied nanofillers include one dimensional carbon nanotubes (CNTs) and two dimensional graphene nanoplateles (GNPs) [3,6–10]. In particular, CNTs stand out as highly conductive fillers in polymer matrices, but they show a clear tendency to form agglomerates and their fabrication is limited to rather expensive approaches, such as chemical vapor deposition and arc discharge methods, which generally are combined with a post-production purification step [11,12]. On the other hand, much easier processing is required for GNPs [13].

Poly(vinylidene fluoride) (PVDF) is an interesting polymer characterized by good mechanical and chemical properties, weather resistance, and more remarkably by unique piezoelectric and ferroelectric properties, which are closely associated with its polar crystalline forms [14,15]. Moreover, PVDF has been widely applied in microfiltration, ultra-filtration, protein adsorption, immobilization and separation, waste water treatment, proton and ionic conductivity [12,16–20], and controlled release of drugs [21]. These properties and applications depend on PVDF crystalline structure. In particular, five different polymorphs have been observed, namely α, β, γ, δ and ε phases, with α and β being the most common allotropes [14,16,21]. The

* Corresponding authors at: Dept. of Astronautical, Electrical and Energy Engineering, Sapienza University of Rome, via Eudossiana 18, 00184 Rome, Italy.
E-mail addresses: hossein.cheraghibidsorkhi@uniroma1.it (H.C. Bidsorkhi), alessandrogiuseppe.daloia@uniroma1.it (A.G. D'Aloia).

http://dx.doi.org/10.1016/j.mtcomm.2017.04.001
Received 15 November 2016; Received in revised form 5 March 2017; Accepted 3 April 2017
Available online 19 April 2017

existence of multiple crystalline structures for PVDF is attributed to the atomic radii of hydrogen and fluorine atoms in the ($-CH_2-CF_2-$) repeating unit, which permit chain polarization [22–24]. The α-phase is characterized by a monoclinic unit cell with Trans–Gauche–Trans–Gauche (TGTG) chain conformation and it is generally formed during crystallization from the melt [23]. On the other hand, the piezo- and pyro-electrically active β-phase with an orthorhombic unit cell in Trans–Trans (TT) conformation can only be obtained after a long and complex processing route. Since in this conformation fluorine and hydrogen atoms are on the opposite sides of the polymer backbone, a net non-zero dipole moment is formed [22], making PVDF a good piezo- and pyroelectrically active polymer [25]. In its β-phase form, PVDF can be used in polymer sensors, actuators, transducers and other electrical and optical applications [26–28]. The β-phase of PVDF is generally obtained through uniaxial or biaxial stretching of melt-crystallized films [29], melt crystallization under high pressure [30], crystallization from solution under special conditions [31] or through the application of high electric fields to PVDF in its α-phase [32]. Numerous studies have also demonstrated that the addition of external nucleating agents such as modified CNTs [33] and functionalized GNPs [34,35] or clay particles [36] can induce β-phase formation in PVDF nanocomposites obtained by solution casting. However, in these cases the formation of a piezoelectric β-phase is achieved only after modifications of the filler surface to improve its capability to adsorb PVDF chains. In fact, the high adhesion achieved at the PVDF-filler interface causes a transformation of the α-phase TGTG conformation into the β-phase TT conformation. Moreover, functionalized GNPs can also be used as nucleating agent for PVDF, to produce high performance composites film materials [35]. Nevertheless, it should be pointed out that one important issue is that chemical modifications are performed in general applying expensive methods, which are unfriendly from environmental point of view and make large use of toxic organic solvents and acids. Actually, graphene, when used in polymers as nanofiller, is typically subjected to chemical modifications in order to better affect polymer chain orientation and morphology.

In the past, the authors investigated the electrical, electromagnetic, mechanical and electromechanical properties of GNP-filled nanocomposites [6,8,13,37–41]. In particular, based on the remarkable physical, electrical and electromagnetic properties of GNPs, economically viable polymer nanocomposites with good electrical and mechanical properties have been produced.

The aim of the present work is to produce and characterize composite films of PVDF filled with different weight concentrations of GNPs through a solution casting method, without any chemical modification or functionalization, either on GNPs or on polymer chains. In particular, this work can open new perspectives in the use of graphene as nanofiller in polymer composites, when researchers want to avoid chemical modification or functionalization of graphene but, nonetheless, to use graphene in order to affect polymer structure and polymer chain orientation.

Therefore, we investigate the effect of unmodified and unfunctionalized GNPs on the morphology and structure of the produced composite films. To this purpose, scanning electron microscopy (SEM), Atomic Force Microscopy (AFM), X-ray powder diffraction (XRPD), differential scanning calorimetry (DSC), Fourier Transform Infrared Spectroscopy (FTIR) investigations have been carried out. The resulting composites were characterized in terms of β-polymorph formation and porosity, as well as their mechanical, electrical and electromechanical properties. To the best of our knowledge, this is the first study focused on the use of GNPs without any chemical modification or functionalization as nucleation agents for β-phase formation enhancement. The GNP effects on PVDF porosity, morphology and crystal structure is also studied in details. Finally, the produced PVDF/GNP composite films are characterized in terms of electrical, mechanical and electromechanical properties, enabling their use in several engineering fields, such as structural sensing and monitoring.

2. Experimental

2.1. GNP synthesis and composite production

GNPs were produced through thermal expansion of a graphite intercalation compound (GIC) [37]. The starting GIC is characterized by a declared mean lateral size of 350 μm. GIC underwent a thermal shock driven expansion in air at 1150 °C for ~5 s, increasing its volume by roughly 200 times, obtaining thermally expanded graphite oxide (TEGO), also known as worm-like graphite.

The PVDF/GNP composite films were then fabricated via a solution mixing method. Briefly, PVDF was firstly dissolved in *N,N*-dimethylformamide (DMF) through 2 h-magnetic stirring at 65 °C. Successively, TEGOs were mixed in a PVDF-DMF solution, and the obtained dispersion was tip sonicated using a pulsed cycle running for 20 min, thus obtaining a homogeneous suspension of GNPs in the polymer mixture. The obtained solution mixture was casted onto a glass plate. Finally, the samples were put in oven for 8 h at 80 °C.

The weight concentration of the produced PVDF/GNP composite films was 2, 3, 4 and 5%.

2.2. Morphological, structural and thermal characterization

The morphology of the commercial GICs and of the produced TEGOs, GNPs and composite specimens was analyzed through SEM, AFM, XRPD, DSC investigations, all carried out at the Sapienza Nanotechnology and Nanoscience Laboratory (SNN-Lab) and at the Dept.s of Earth Sciences and Chemical Engineering Materials and Environment of Sapienza University of Rome.

SEM images have been acquired through a Zeiss Auriga Field Emission (FE)-SEM. The film composite samples were fractured in liquid nitrogen and when necessary a 10 nm-Cr coating was sputtered on the fracture surfaces using a Quorumteach Q150T sputter coater.

AFM analysis was obtained by using a Bruker-Veeco Dimension Icon AFM. The AFM micrographs were acquired in tapping mode, considering for all the samples a scanning surface area A of 50 μm × 50 μm. Then, the images were analyzed by using the Mountains Map 7 software, allowing the evaluation of several roughness parameters, such as the maximum surface height S_z, the arithmetic mean height S_a, and the root mean square height S_q. The S_z parameter is given by:

$$S_z = S_p + |S_q| = S_p - S_q \tag{1}$$

being S_p the height of the highest point and S_q the height of the lowest point of the surface area A, both counted from the mean plane [42,43].

The arithmetic mean height S_a is the arithmetic mean of the absolute value of the heights h with respect to the mean plane within the sampling area A, i.e.:

$$S_a = \frac{1}{A}\iint_A |h(x, y)|dxdy \tag{2}$$

More statistically significant, the root mean square height S_q is the root mean square value of the surface heights h:

$$S_q = \sqrt{\frac{1}{A}\iint_A |h(x, y)|^2 dxdy}. \tag{3}$$

XRPD data were collected on a Bruker AXS D8 Advance operating in θ/θ geometry in transmission mode on samples prepared as capillaries. The instrument is fitted with incident beam focusing Göbel mirrors and a PSD VÅntec-1D. Sheets of the various samples were reduced to small fragments using a very sharp cutter. The resulting chips were loaded in 1 mm diameter SiO_2-glass capillaries that were kept open at one side. GNPs were gently ground in an agate mortar to produce a powder that was loaded in a 0.7 mm diameter SiO_2-glass capillary. Capillaries were mounted on standard goniometer heads and aligned along the beam-path. Data were collected in the 5°–90° 2θ angular range, 0.022° 2θ step size, 2 s counting time. Calculated diffraction patterns of β and α PVDF

polymorphs were obtained from the structural data of Hasegawa et al., 1972 and Takahashi et al., 1983 respectively, using the GSAS suite of programs and the EXPGUI graphical user interface [23,44,45].

Finally, the crystallinity and the melting behaviour of PVDF and PVDF/GNP composite films were evaluated using a DSC test, using a SDT Q600 (TA Instruments) in nitrogen atmosphere and heating 10 mg of samples from 30 °C to 300 °C. The crystallinities of PVDF and PVDF/GNP film composites was calculated as:

$$X_c = \frac{\Delta H_m}{\Delta H_m^0\, \omega} \cdot 100 \tag{4}$$

where X_c is the sample crystallinity expressed in %, ΔH_m is the sample enthalpy at melting point obtained by heating process, ΔH_m^0 is the reference melting enthalpy of pure PVDF (104,6 J/g) when the crystallinity is 100% [46], and ω is the amount of PVDF weight fraction in composites.

2.3. Sheet resistance measurement

The sheet resistance R_S was measured by applying the four-wire volt-amperometric method to the produced PVDF/GNP composite films.

At first, each PVDF/GNP film was cut obtaining a rectangular sample. The opposite sides of each film were coated with silver conductive paint (Electrolube®) to provide two rectangular contacts, as shown in Fig. 1(a). Then, tin-coated copper wires were bonded to the aforementioned contact pads using a bi-component Ag-filled epoxy adhesive (Circuitworks®). Subsequently, the samples were cured in oven at 120 °C for 10 min. The produced samples were electrically characterized using a Keithley 6221 dc/ac current source connected to a Keithley 2182a nano-voltmeter, controlled by a laptop.

Since the surface between the silver electrical contacts is a square of side l, the effective dc electrical conductivity of each sample γ_S was extracted from the measured resistance value R_S as:

$$\gamma_S = (tR_S)^{-1} \tag{5}$$

where t is the thickness of the sample.

2.4. Mechanical and electromechanical characterization

An INSTRON 3366 universal testing machine equipped with a 500 N load cell was used to perform the mechanical tensile tests of the produced PVDF/GNP composite films. The specimens to be tested were realized following a modified version of the standard ASTM D 882. To this purpose, each PVDF/GNP film was cut into rectangular strips. The top and bottom parts of the rectangular strips were inserted between the grips of a screw action tensile test fixture, having two conducting plates as electrodes. These parts represent the contact areas and are marked with white lines in Fig. 1(b). Then, the resistance values were measured with the same current source and nano-voltmeter previously used (Section 2.3). It should be noted that in this configuration the measured resistance, represents the total volume resistance of the sample because the metallic grips, acting as electrodes, penetrate the sample surface. Conversely, in the sheet-resistance measurement described in Section 2.3, the silver contacts are deposited over the sample surface, so that the resulting value of resistance in mainly representative of the conducting properties of the sample surface.

Therefore, the effective conductivity γ_{eff} of the composite film was extracted by applying the following expression:

$$\gamma_{eff} = a\,(ctR_0)^{-1} \tag{6}$$

in which R_0 is the initial resistance of the sample under test, the d.c. electrical resistance measured without any applied mechanical tensile stress, a is the distance between the contact areas (Fig. 1(b)), c and t are respectively the width and the thickness of the specimen.

The piezoresistive response of the PVDF/GNP composite films was then characterized by measuring the variation of the dc electrical resistance R due to the applied tensile stress, i.e:.

$$\Delta R/R_0 = (R - R_0)/R_0. \tag{7}$$

in which R is the electrical resistance corresponding to the generic strain ε.

The same experimental set-up has been used to measure the maximum tensile strength, the corresponding strain, and to extrapolate the Young's Modulus.

2.5. Fourier transform infrared spectrometer (FTIR)

All the FTIR absorption spectra were recorded using a FT-IR spectrometer (Vertex 70 by Bruker Optics GmbH) equipped with a single reflection diamond ATR cell. The analyses were performed into the typical Mid IR spectral range (4000–400 cm^{-1}) at a resolution of 2 cm^{-1} and with 256 scans.

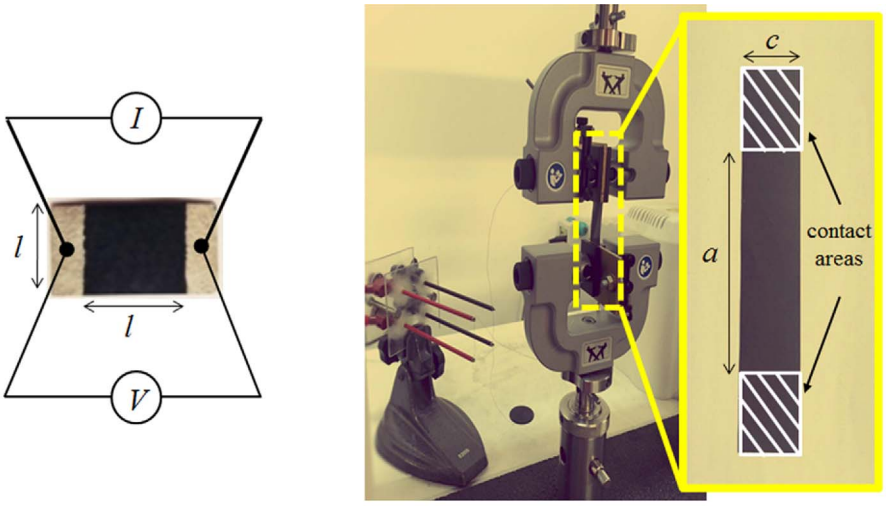

Fig. 1. (a) GNP based composite films prepared for sheet resistance measurement and (b) electro-mechanical measurement set-up. (l = 1 cm, a = 20 cm, c = 2 cm).

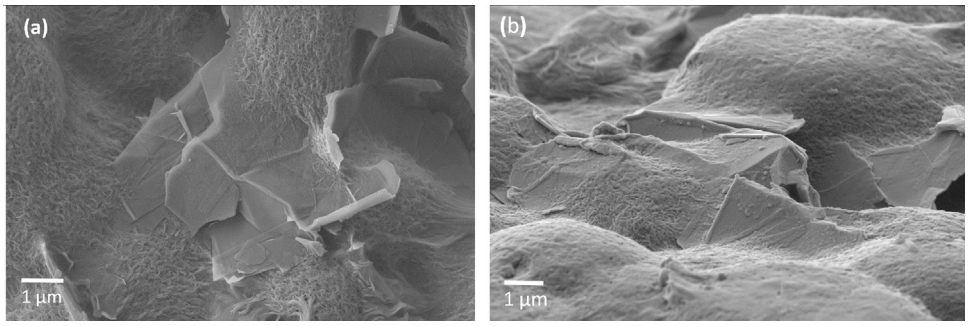

Fig. 2. SEM micrographs at different magnifications of the tilted top surface view of PVDF/GNP composite films with (a) 2% wt and (b) 5% wt GNPs, showing good adhesion between GNPs and the polymer matrix.

3. Results and discussion

3.1. Morphology

Figs. 2 and 3 show the SEM cross-section and surface images of the produced PVDF and PVDF/GNP composite film samples.

A good integration between the GNPs and the polymer matrix is achieved, as it can be observed in Fig. 2(a) and (b), showing PVDF composites filled with GNPs at 2% wt and 5% wt, respectively. In particular, in both cases the GNP surface is almost entirely covered by the PVDF polymer matrix. Moreover, the PVDF polymer chains seem to have a good adhesion with the GNPs, as pointed out by Fig. 2(a) and (b).

Fig. 3(a) and (b) shows the surface of a neat PVDF film, characterized by a spherulitic structure with high porosity and large spherical particles. When a little amount of GNP is added, the spherulitic PVDF structure does not change, but the average lateral dimensions of pores and spherical particles become smaller, as can be noticed in Fig. 3(c)–(d), showing the SEM surface image of a PVDF composite film filled with 2% wt of GNPs. This is attributed to PVDF-GNP adhesion and to the GNP dispersion in the polymer matrix [47].

When the GNP concentration increases, the PVDF/GNP composite film morphology changes significantly from the initial semi-spherulitic structure to a more compact configuration. In fact, for GNP concentration higher than 3% wt, the film porosity decreases noticeably with respect to the one observed on samples of neat PVDF and of PVDF/GNP loaded at 2% wt. This change can be observed in Fig. 3(e) and in its magnification (Fig. 3(f)), showing a PVDF composite film filled with 3% wt of GNPs. As the GNP content increases to 4% wt (Fig. 3(g)–(h)) and to 5% wt (Fig. 3(i)(j)), the film porosity strongly decreases. In particular, looking at Fig. 3(i) and at its magnification (Fig. 3(j)), it can be noticed that almost 70% of the original pores are closed by GNPs, as pointed out in Fig. 3(j). In fact, it has been found that GNPs have a nucleation effect on the PVDF structure, constraining the polymer chains to orient in such a way to facilitate the β phase formation and to close pores [47–49].

These observations are in line with experimental DSC, AFM, electrical, mechanical and electromechanical characterizations, as it is reported in the following.

3.2. AFM

The AFM topographical images of the PVDF and PVDF/GNP composite film surfaces are shown in Fig. 4. Table 1 summarizes the surface areas and roughness parameters, extracted upon AFM micrograph post-processing.

Fig. 4(a) and (b) shows the AFM topographies of neat PVDF film sample, named PG0. The brightest regions represent areas of the film surfaces with maximum height, whereas the darkest regions correspond to the pores or valleys [50]. In particular, Fig. 4(a) shows the top surface of a spherulite, and Fig. 4(b) the valley between two adjacent spherulites. The estimated values of roughness of the observed surface areas are reported in Table 1. It results that the values of the roughness parameters estimated using data of Fig. 4(a) are much lower than the ones obtained from Fig. 4(b), since the former picture is centered on a spherulite covering almost all the scanning area A, whereas the latter one is focused on a valley between two adjacent spherulites. We can also observe that the PVDF spherulite diameter is greater than 50 μm, since it covers all the scanning area of Fig. 4(a).

In PVDF/GNP composite films, we notice a significant reduction of spherulites diameter, roughness and pores size. In particular, looking at sample PG2, filled with 2% wt of GNP (Fig. 4(c)), we notice that the spherulite diameter is lower than 10 μm. Moreover, sample PG3 and PG4, respectively filled with 3% wt and 4% wt of GNP, are characterized by spherulites with diameter lower than 10 μm and 5 μm, respectively. Finally, we notice that when 5% wt of GNP is added to PVDF (i.e. sample PG5 shown in Fig. 4(f)), the roughness is much lower in comparison with the one of the samples with a lower GNP content: actually, there are almost no pores and the spherulite diameter is generally lower than 2 μm. As a consequence, the addition of GNPs causes a significant reduction of spherulite diameter, roughness and pores size of the composite film. These results may confirm a nucleation effect of GNP in the polymer chains and a phase changing in the polymer structure.

3.3. DSC analysis

Fig. 5 and Table 2 show the results of the DSC analyses performed on the neat PVDF and on the PVDF/GNP composite films. Looking at the thermograph of Fig. 5, it is evident that the melting point T_m increases significantly as the GNP content increases. Moreover, DSC shows a considerable change in the crystallinity of the composite film when GNP is added. In particular, as reported in Table 2, when 2% wt of GNP is added, the crystallinity rises to 37.61%.

Nevertheless, sample PG3 shows a slight decrease in crystallinity with respect to sample PG2, probably due to the GNP nucleation effect on polymer matrix. In fact, due to the presence of GNPs, the polymer chains tend to join together, causing a decrease in crystallinity and porosity [51]. For higher GNP concentration (4% wt and 5% wt), an increase in crystallinity is noticed. In particular, the crystallinity rises to nearly 40% in the sample PG5.

3.4. XRPD analysis

The crystal structure of PVDF and PVDF/GNP composite films was investigated by powder XRPD diffraction. Fig. 6 illustrates the XRPD analysis of composite films filled with different amounts of GNPs. According to recent studies [52,53], the characteristic peaks of PVDF are at 2θ = 17.76, 18.42, 20.00, 25.69, 26.68, 32.35, 33.14, 35.96 and 38.70, which are, respectively, allocated to the (120) (021) (121) (130) (210), and (002) planes. All these peaks refer to α-phase of pure PVDF polymer, while the major crystalline peak for α-phase of PVDF are

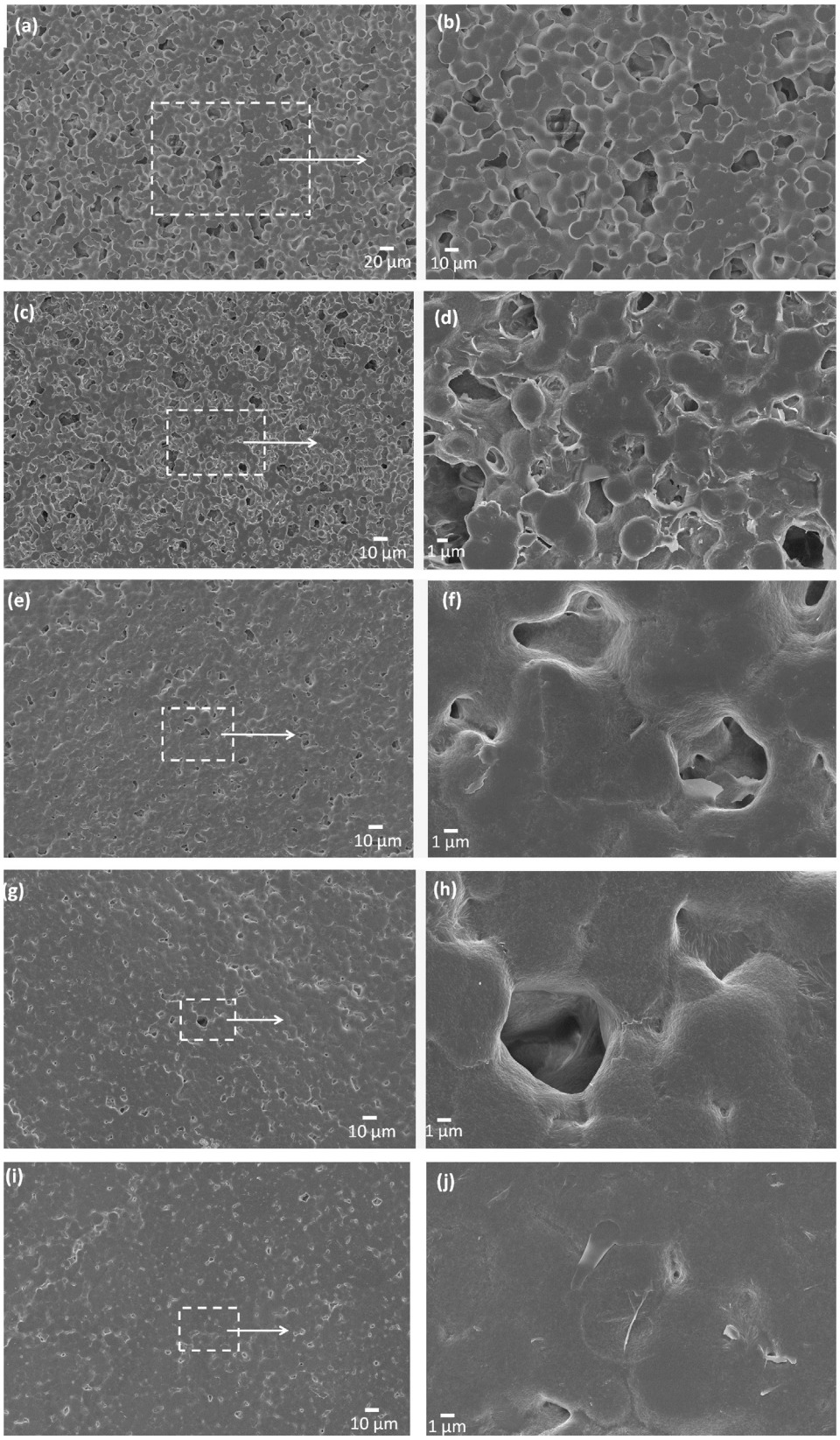

Fig. 3. SEM micrographs at different magnifications of the surface of the (a)–(b) neat PVDF and PVDF/GNP composite films with (c)–(d) 2 wt%, (e)–(f) 3 wt%, (g)–(h) 4 wt%, and (i)–(j) 5 wt%. These images show the GNP effect on the structure and porosity of PVDF/GNP composites films.

located at (100) (020) and (110) planes.

It is noticed that the XRPD spectra change when GNP is added to PVDF. In particular, the same α-phase peaks at (120), (121) and (130) planes disappeared, and the intensity of other α-phase peaks strongly decreased and became broad.

It is also interesting to note that the (100) peak almost disappeared, the intensity of (020) peak significantly dropped, and the important peak at $2\theta = 20^{\circ}$ shifted to $2\theta = 20.4^{\circ}$ and became wide broad. The

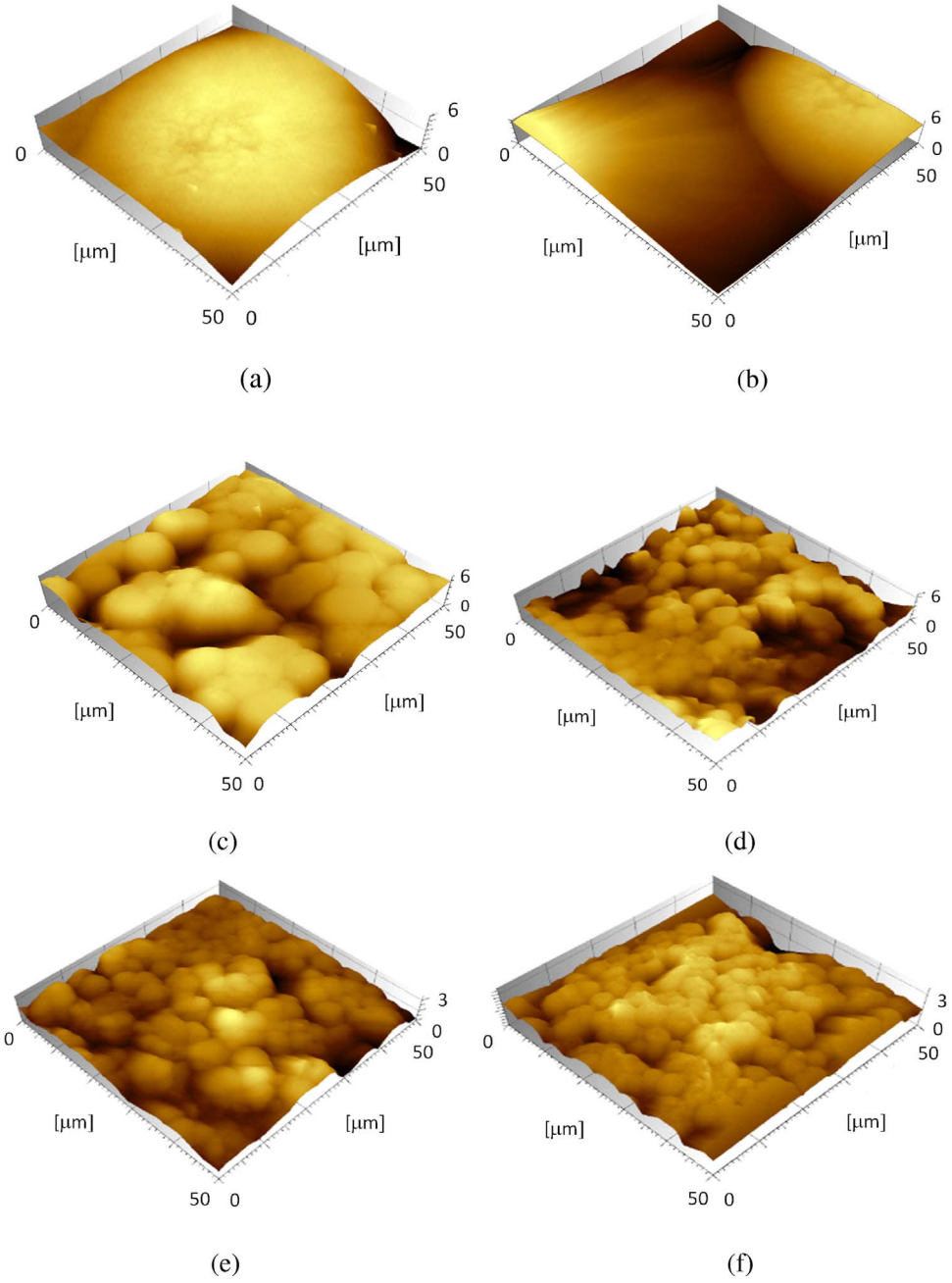

Fig. 4. Three-dimensional surface images of the PVDF (a) (b) and PVDF/GNP composites with 2 wt% (c), 3 wt% (d), 4 wt% (e), and 5 wt% (f) of GNPs.

Table 1
Surface parameters of the PVDF (a) (b) and PVDF/GNP composites with 2 wt%, 3 wt%, 4 wt%, and 5 wt% of GNPs, estimated from the data shown in Fig. 7(a)–(f), respectively.

Figure	Sample name	GNP concentration [% wt]	Measured surface area [μm^2]	Roughness parameters		
				S_a [μm]	S_q [μm]	S_z [μm]
4(a)	PG0	0	2531	0.456	0.591	3.59
4(b)	PG0	0	2579	1.130	1.400	5.77
4(c)	PG2	2	2997	0.725	0.890	4.67
4(d)	PG3	3	3107	0.697	0.783	4.13
4(e)	PG4	4	2561	0.290	0.365	2.50
4(f)	PG5	5	2597	0.250	0.321	2.38

peak shifting is due to (110) and (200) planes of β-phase, implying that the GNP help the α-phase transformation of PVDF into β-phase.

Thus, we can conclude that the GNPs act as platforms for nucleation sites. In fact, as the GNP amount increases, the β-phase formation becomes more evident [49,54–56].

The calculated patterns of the α- and β-phases are reported in Fig. 7. From a visual inspection of the data reported in Fig. 6, it is clearly apparent that the XRDP spectra of the GNP-loaded samples can be interpreted as arising from linear combinations of the diffraction patterns of these two phases. [23,44,45].

3.5. FTIR analysis

Fig. 8 shows the FTIR results obtained from pure PVDF films and PVDF/GNP composite films. In the case of pure PVDF, the vibration bands are observed at 484 cm^{-1} (−CF2 wagging), 531 cm^{-1} (−CF2 bending), 614 cm^{-1} (skeletal bending), 762 cm^{-1} (−CF2 bending),

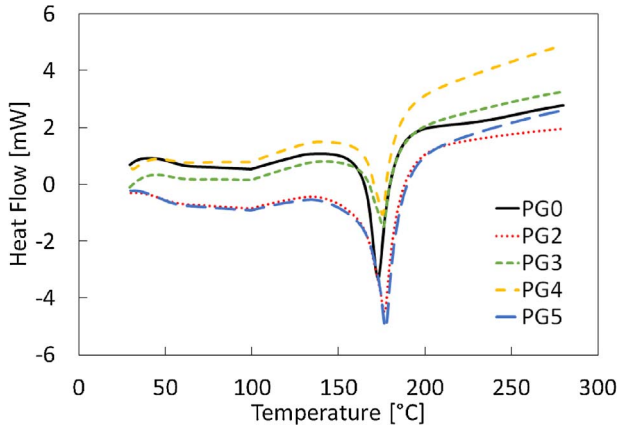

Fig. 5. DSC curve of PVDF and PVDF/GNP composite films containing different amounts of GNP.

Table 2
Summary of DSC carves of PVDF and PVDF film composites.

Sample	GNP concentration [% wt]	T_m [°C]	Crystallinity [%]
PG0	0	172.92 °C	29.46
PG2	2	176.67 °C	37.61
PG3	3	175.90 °C	32.09
PG4	4	175.53 °C	34.02
PG5	5	177.26 °C	39.92

794 cm^{-1} (−CH2 rocking) and 973 cm^{-1} (twisting), i.e. in the FTIR spectra assigned to the PVDF α-phase, as reported in [57]. When GNPs are added to the composite films, the intensity of the previous peaks decreases noticeably and absorbance bands with strong intensity at 509 cm^{-1} (−CF2 stretching) and 840 cm^{-1} (−CH2 rocking, −CF2 stretching and skeletal C−C stretching) appear. The last absorbance bands are related to the PVDF *β*-phase. The phase transformation from α-phase to *β*-phase is attributed to GNP force (or stress field) applied to nucleation sites in polymer structure [48,49,52,58].

3.6. Sheet resistance and dc electrical conductivity

Fig. 9(a) reports the sheet resistances R_S of the produced samples, measured as explained in Section 2.3. These data are compared with the values of the resistance R_0 measured during the electromechanical characterization (as described in Section 2.4) when no load is applied. Moreover, Fig. 9(b) shows the conductivities γ_S and γ_{eff}, computed

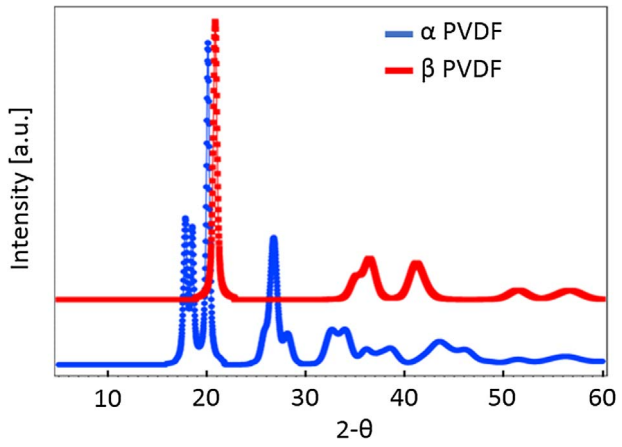

Fig. 7. XRPD simulated patterns of β and α phase of a PVDF/GNP composite films.

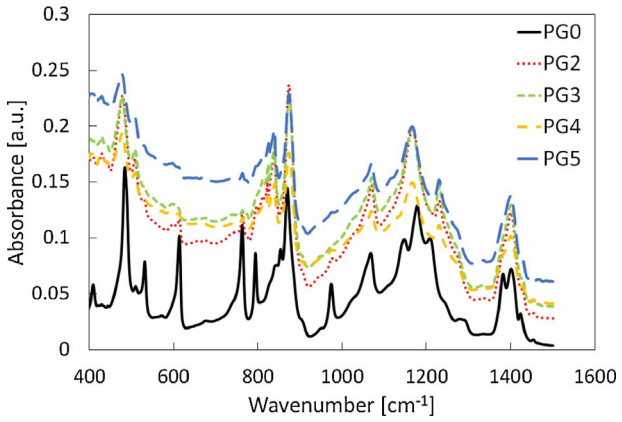

Fig. 8. FTIR curve of PVDF and PVDF/GNP composite films containing different amounts of GNP.

respectively from the measured values of R_S and R_0, using Eqs. (5) and (6).

It can be noticed that the sheet resistance R_S of sample PG2 is much higher than the corresponding bulk resistance R_0. This is due to the fact that at low filler concentration, GNPs are well embedded in the polymer matrix and do not emerge over the film surface. As a consequence, the sheet resistance R_S is greater than the volume resistance R_0, because the silver coated rectangular patches shown in Fig. 1(a) enable to contact only the sample surface. On the other hand, the metallic grips used to

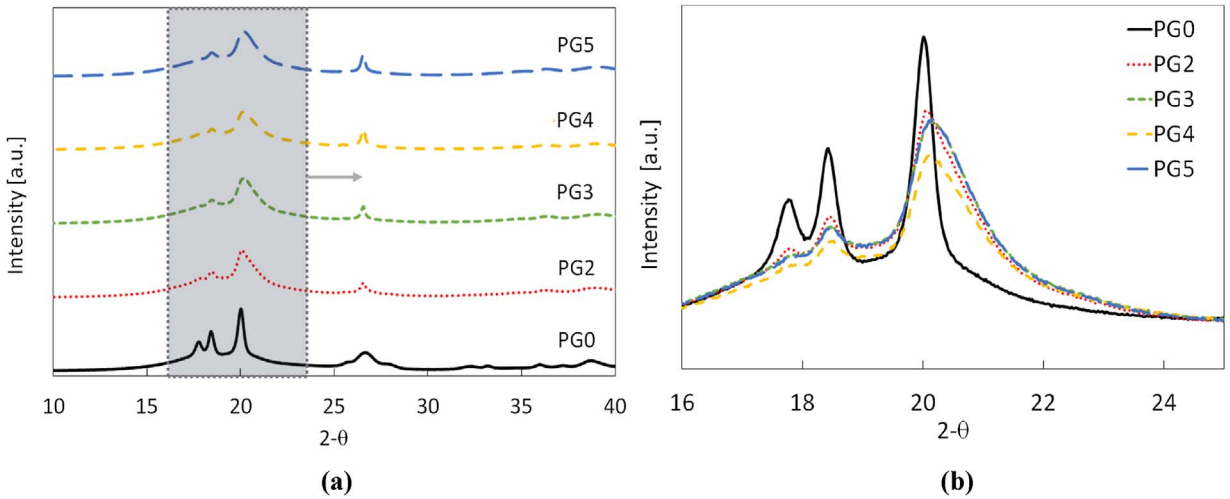

Fig. 6. XRPD patterns of PVDF and PVDF/GNP composite films containing different amounts of GNP.

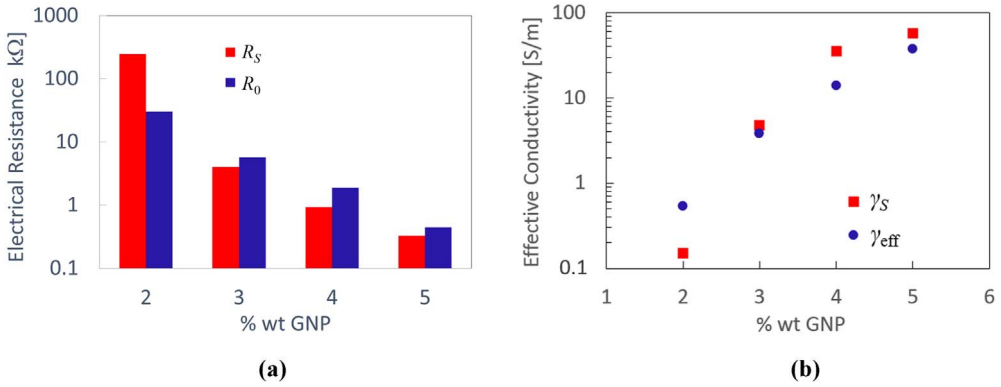

Fig. 9. (a) Sheet resistances R_S and volume resistances R_0 of the produced samples and (b) corresponding conductivities γ_S and γ_{eff} as function of the GNP weight concentration.

hold and contact the sample in the electromechanical characterization set up enable to contact both the surface and the inner volume of the specimen. As the GNP concentration increases, the porosity decreases since the pores are closed by the GNPs. Therefore, the conducting fillers tend to emerge over the film surface, providing a better electrical contact with the silver coated rectangular strips. This is confirmed by the data reported in Fig. 9(a) and by the extracted conductivities if Fig. 9(b).

3.7. Mechanical properties

Fig. 10 reports the measured tensile stress-strain characteristic of the produced PVDF and PVDF/GNP composite films, whose mechanical properties are summarized in Table 3. When 2% wt of GNP is added, the Young's modulus of the PVDF/GNP composite films increases of about 20% while the tensile strength and the percentage strain at break slightly reduce. This is indicative of good adhesion and dispersion of GNPs into the polymer matrix [57], as confirmed by the SEM images shown in Fig. 2.

On the other hand, when the GNP concentration is 3% wt, the measured mechanical properties of the composite decrease slightly with respect to the ones of the 2% PVDF/GNP composite. This decrease is due to the morphology change previously observed through SEM and AFM characterizations. In fact, the porosity of the composite film reduces due to the addition of GNPs and to the consequent change in polymer chains orientation and organization, giving rise to a semi-spherulitic structure. As the GNP amount further increases, the number of pores covered by GNPs increases and the mechanical properties slightly improve. In fact, the composites morphology show a non-spherulitic structure with low porosity, as pointed out in Section 3.2. This new composite morphology is originated by the GNP nucleation

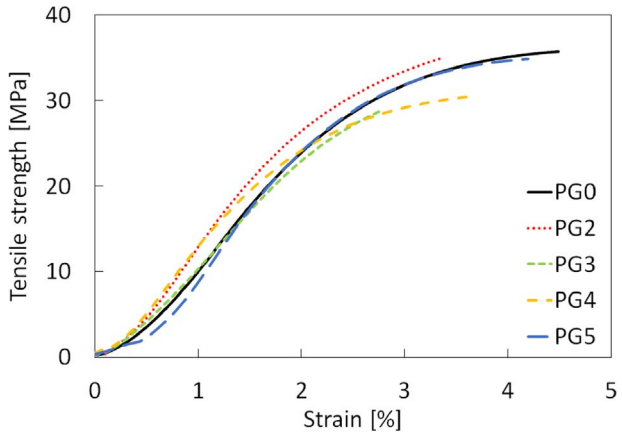

Fig. 10. Measured tensile stress-strain characteristic of the produced samples having the mechanical properties reported in Table 3.

Table 3
Mechanical properties of PVDF and PVDF/GNP composite films containing different amounts of GNP.

Samples	Tensile Strength [MPa]	Young's Modulus [GPa]	Strain at Break [%]
PG0	35.4	1.56	4.1
PG2	34.8	1.85	3.3
PG3	28.8	1.35	2.7
PG4	30.4	1.42	3.6
PG5	34.8	1.78	4.1

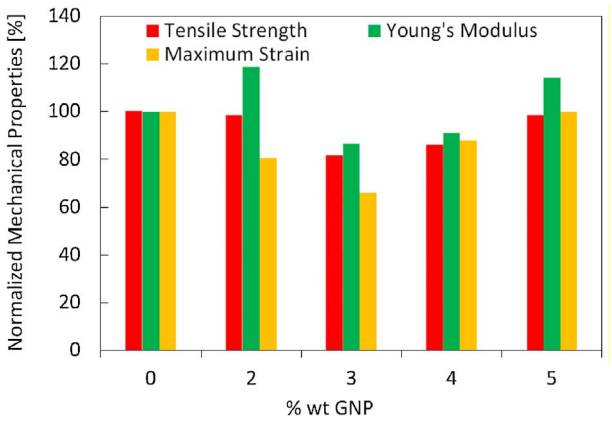

Fig. 11. Normalized tensile strength, Young's modulus and strain at break as a function of the GNP concentration.

effect on PVDF chains, since GNPs force the polymer chains to orient themselves and reduce porosity.

The variation of the tensile strength, Young's modulus and strain at break as a function of GNP concentration is highlighted in the histogram of Fig. 11, where such mechanical properties are normalized with respect to the ones of pure PVDF.

3.8. Electromechanical properties

The resistance measured as a function of the applied tensile strain of the samples is shown in Fig. 12(a). Fig. 12(b) shows the variation of the dc electrical resistance with respect to the initial value R_0 as a function of the strain. The curves obtained under a quasi-static tensile loading show a rapid nonlinear increase of the resistance with the induced strain and, as expected, the highest values of resistance are obtained for the samples loaded with 2% wt of GNPs. The piezoresistive phenomenon can be mainly attributed to modifications of the conducting nanofiller network inside the composite, due to the increase of inter-flake distances during loading [39], which can produce change of the tunneling resistance in neighboring GNPs and loss of contact between

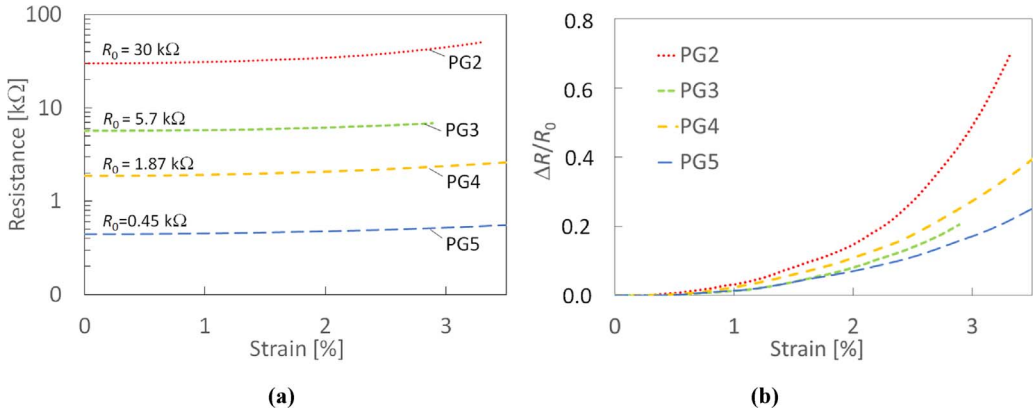

Fig. 12. Measured dc resistance as function of the induced strain (a) and its variation with respect to the intial value R_0 (b), for the composite samples PG0, PG2, PG3, PG4 and PG5.

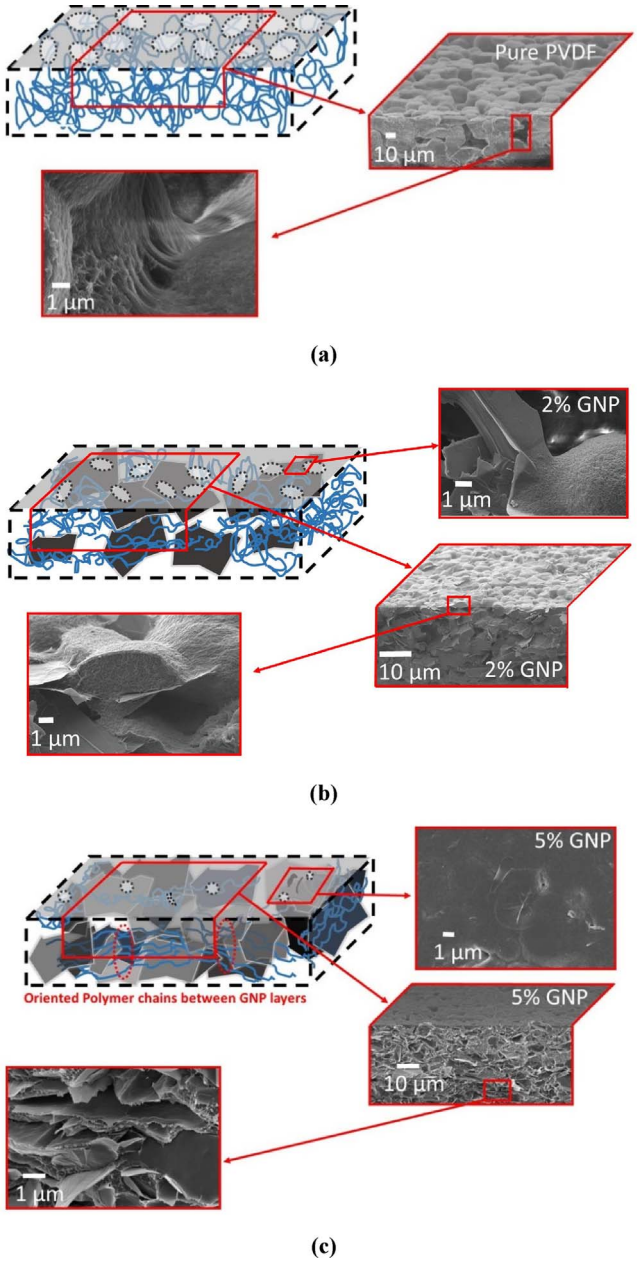

Fig. 13. Polymer structure scheme of (a) pure PVDF film with not oriented polymer chains, (b) PVDF/GNP composite film with low GNP concentration and partially oriented polymer chains and (c) PVDF/GNP composite film with high GNP concentration and oriented polymer chains.

adjacent nanofillers.

4. GNP effect on porosity and β-phase formation

The pure PVDF film is characterized by a spherulitic structure with high porosity and large spherical particles, as schematically sketched in Fig. 13(a). When a little amount of GNP is added, the spherulitic PVDF structure does not change, but the average lateral dimensions of pores and spherical particles become smaller, as represented in Fig. 13(b). This mechanism is attributed to the adhesion of PVDF to GNP flakes and to the GNP dispersion in the polymer matrix [47].

When the GNP concentration increases, the PVDF/GNP composite film morphology changes noticeably and the porosity decreases. In fact, the GNP flakes tend to close most of the pores, and the polymer chains seem to be more oriented, as observed in the SEM images previously shown and as sketched in the scheme of Fig. 13(c).

This is due to the fact that GNPs facilitate the alignment of polymer chains between the GNPs, as shown in the SEM image of Fig. 14(a) and in the corresponding scheme. This alignment facilitate the β-phase formation, as it has been found from XRD and FTIR results. This experimental evidence can be attributed to electrostatic charge localization over the GNP surface. In fact, during the production process, electrostatic charges may accumulate on the GNP surfaces due to ultrasonication, magnetic mixing and curing steps. As a consequence, a weak electrostatic field occur between the surface of adjacent GNPs. The positive hydrogen atoms are attracted to the GNP surface with negative electrostatic charge, as sketched in Fig. 14(b). On the other hand, the negative fluorine atoms are attracted to the GNP surface with positive electrostatic charge. Then, the ($-CH_2-CF_2-$) PVDF polymer chains assume the form shown in Fig. 14(b), corresponding to the β-phase.

5. Conclusions

In this study, PVDF/GNP composite films with GNP content of 2, 3, 4 and 5% wt were produced, and their porosity, crystallinity and morphology were investigated. The FTIR and XRD spectra show the transition from α-phase to β-phase, as evidenced by the broadening and upshift of the (121) XRD peak from 20° θ to 20.4° θ. Moreover, α-phase peaks in FTIR spectra significantly decrease its amplitude, while the intensity of β-phase peaks at 840 $cm^{-1}$and 509 cm^{-1} is enhanced. The porosity and large spherical particles are extremely reduced by adding GNPs into the PVDF matrix, as it can be noticed from SEM and AFM characterizations. The electrical, mechanical and electromechanical properties of the produced composite films depend clearly on GNP concentration and polymer morphology. In fact, when 2% wt of GNP is added to the polymer matrix, a good adhesion and dispersion of GNPs into the polymer matrix is noticed and the Young's modulus increases while the tensile strength and the percentage strain at break slightly

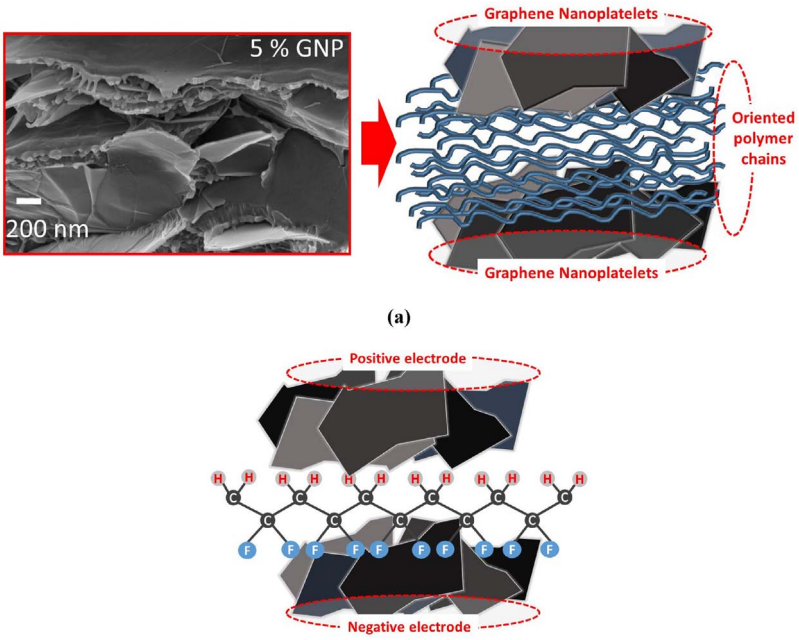

Fig. 14. (a) Polymer chains aligned between GNPs in PVDF/GNP composite film with high filler concentration and (b) *β*-phase formation among adjacent GNPs surfaces.

reduce. At the same time, we observe that the sheet resistance of the produced samples decreases with the GNP filler content. Moreover, the sample filled with GNPs at 2% wt is characterized by the highest sensitivity with respect to an induced strain.

For higher GNP amounts, the polymer chains change orientation and organization. As the GNP content further increases, a slight improvement of mechanical properties is noticed due to polymer chains orientation. All the achieved results demonstrate that GNPs act as nucleation sites on the polymer phase, and influence as a physical power force the morphology and structure of the molecular and polymer chains, producing a relevant reduction of the GNP/PVDF composite film porosity, which can be tuned through the proper setting of the filler content.

In conclusion, the obtained results open new perspectives in the use of graphene and graphene nanostructures as filler in polymer composite because they demonstrate that it is possible to affect polymer structure and morphology avoiding the use of chemically modified graphene.

References

[1] D.W. Schaefer, R.S. Justice, How nano are nanocomposites? Macromolecules 40 (24) (2007) 8501–8517.
[2] S. Kango, et al., Surface modification of inorganic nanoparticles for development of organic–inorganic nanocomposites—a review, Prog. Polym. Sci. 38 (8) (2013) 1232–1261.
[3] F.-C. Chiu, Y.-J. Chen, Evaluation of thermal, mechanical, and electrical properties of PVDF/GNP binary and PVDF/PMMA/GNP ternary nanocomposites, Compos. Part A: Appl. Sci. Manuf. 68 (2015) 62–71.
[4] H.C. Bidsorkhi, et al., Preparation and characterization of ethylene-vinyl acetate/halloysite nanotube nanocomposites, J. Mater. Sci. 50 (8) (2015) 3237–3245.
[5] M. Soheilmoghaddam, et al., Development of ethylene-vinyl acetate composites reinforced with graphene platelets, Macromol. Mater. Eng. 302 (February (2)) (2017) 1–9.
[6] M.S. Sarto, et al., Synthesis, modeling, and experimental characterization of graphite nanoplatelet-based composites for EMC applications, IEEE Trans. Electromagn. Compat. 54 (1) (2012) 17–27.
[7] J. Tong, H.-X. Huang, M. Wu, Facile green fabrication of well dispersed poly (vinylidene fluoride)/graphene oxide nanocomposites with improved properties, Compos. Sci. Technol. 129 (2016) 183–190.
[8] M. Soheilmoghaddam, et al., Regenerated cellulose nanocomposites reinforced with exfoliated graphite nanosheets using BMIMCL ionic liquid, Polymer 55 (14) (2014) 3130–3138.
[9] Z. Zhang, et al., Enhanced dielectric and mechanical properties in chlorine-doped continuous CNT sheet reinforced sandwich polyvinylidene fluoride film, Carbon 107 (2016) 405–414.
[10] D.Y. Kim, et al., Graphene paper with controlled pore structure for high-performance cathodes in Li–O2 batteries, Carbon 100 (2016) 265–272.
[11] Y. Li, S.C. Tjong, R. Li, Electrical conductivity and dielectric response of poly (vinylidene fluoride)–graphite nanoplatelet composites, Synth. Met. 160 (17) (2010) 1912–1919.
[12] J.-H. Cao, B.-K. Zhu, Y.-Y. Xu, Structure and ionic conductivity of porous polymer electrolytes based on PVDF-HFP copolymer membranes, J. Membr. Sci. 281 (1–2) (2006) 446–453.
[13] A. D'Aloia, et al., Electromagnetic absorbing properties of graphene–polymer composite shields, Carbon 73 (2014) 175–184.
[14] A. Lopes, et al., Nucleation of the electroactive γ phase and enhancement of the optical transparency in low filler content poly (vinylidene)/clay nanocomposites, J. Phys. Chem. C 115 (37) (2011) 18076–18082.
[15] R.K. Layek, et al., Enhancement of physical, mechanical, and gas barrier properties in noncovalently functionalized graphene oxide/poly(vinylidene fluoride) composites, Carbon 81 (2015) 329–338.
[16] S. Yu, et al., Formation mechanism of β-phase in PVDF/CNT composite prepared by the sonication method, Macromolecules 42 (22) (2009) 8870–8874.
[17] M. Rezaei, et al., Preparation and characterization of PVDF-montmorillonite mixed matrix hollow fiber membrane for gas–liquid contacting process, Chem. Eng. Res. Des. 92 (11) (2014) 2449–2460.
[18] H. Adelnia, et al., Gas permeability and permselectivity properties of ethylene vinyl acetate/sepiolite mixed matrix membranes, Sep. Purif. Technol. 146 (2015) 351–357.
[19] D.-a. Zha, et al., Superhydrophobic polyvinylidene fluoride/graphene porous materials, Carbon 49 (15) (2011) 5166–5172.
[20] Y. Cui, S.I. Kundalwal, S. Kumar, Gas barrier performance of graphene/polymer nanocomposites, Carbon 98 (2016) 313–333.
[21] A.J. Lovinger, Annealing of poly (vinylidene fluoride) and formation of a fifth phase, Macromolecules 15 (1) (1982) 40–44.
[22] A. Nandi, L. Mandelkern, The influence of chain structure on the equilibrium melting temperature of poly (vinylidene fluoride), J. Polym. Sci. B: Polym. Phys. 29 (10) (1991) 1287–1297.
[23] R. Hasegawa, et al., Crystal structures of three crystalline forms of poly (vinylidene fluoride), Polym. J. 3 (5) (1972) 600–610.
[24] M. El Achaby, et al., Piezoelectric β-polymorph formation and properties enhancement in graphene oxide–PVDF nanocomposite films, Appl. Surf. Sci. 258 (19) (2012) 7668–7677.
[25] E. Fukada, T. Furukawa, Piezoelectricity and ferroelectricity in polyvinylidene fluoride, Ultrasonics 19 (1) (1981) 31–39.
[26] N. Levi, et al., Properties of polyvinylidene difluoride-carbon nanotube blends, Nano Lett. 4 (7) (2004) 1267–1271.
[27] K. Takashima, et al., Piezoelectric properties of vinylidene fluoride oligomer for use in medical tactile sensor applications, Sens. Actuators A: Phys. 144 (1) (2008) 90–96.
[28] B. Ameduri, From vinylidene fluoride (VDF) to the applications of VDF-containing polymers and copolymers: recent developments and future trends, Chem. Rev. 109 (12) (2009) 6632–6686.
[29] P. Sajkiewicz, A. Wasiak, Z. Gocłowski, Phase transitions during stretching of poly (vinylidene fluoride), Eur. Polym. J. 35 (3) (1999) 423–429.

[30] J. Scheinbeim, et al., High-pressure crystallization of poly (vinylidene fluoride), J. Appl. Phys. 50 (6) (1979) 4399–4405.
[31] R.L. Miller, J. Raisoni, Single crystals of poly (vinylidene fluoride), J. Polym. Sci.: Polym. Phys. Ed. 14 (12) (1976) 2325–2326.
[32] J. Luongo, Far-infrared spectra of piezoelectric polyvinylidene fluoride, J. Polym. Sci. Part A-2: Polym. Phys. 10 (6) (1972) 1119–1123.
[33] S. Manna, A.K. Nandi, Piezoelectric β polymorph in poly (vinylidene fluoride)-functionalized multiwalled carbon nanotube nanocomposite films, J. Phys. Chem. C 111 (40) (2007) 14670–14680.
[34] R.K. Layek, et al., Physical and mechanical properties of poly (methyl methacrylate)-functionalized graphene/poly (vinylidine fluoride) nanocomposites: piezoelectric β polymorph formation, Polymer 51 (24) (2010) 5846–5856.
[35] J. Yu, et al., Graphene nanocomposites based on poly (vinylidene fluoride): structure and properties, Polym. Compos. 32 (10) (2011) 1483–1491.
[36] J. Buckley, et al., Nanocomposites of poly (vinylidene fluoride) with organically modified silicate, Polymer 47 (7) (2006) 2411–2422.
[37] G. De Bellis, et al., Electromagnetic properties of composites containing graphite nanoplatelets at radio frequency, Carbon 49 (13) (2011) 4291–4300.
[38] R.H. Pour, et al., Mechanical, thermal, and morphological properties of graphene reinforced polycarbonate/acrylonitrile butadiene styrene nanocomposites, Polym. Compos. 37 (6) (2016) 1633–1640.
[39] A. Tamburrano, et al., The piezoresistive effect in graphene-based polymeric composites, Nanotechnology 24 (46) (2013) 465702.
[40] J.N. Gavgani, et al., Lightweight flexible polyurethane/reduced ultralarge graphene oxide composite foams for electromagnetic interference shielding, RSC Adv. 6 (33) (2016) 27517–27527.
[41] E. Kovalska, C. Kocabas, Organic electrolytes for graphene-based supercapacitor: liquid, gel or solid, Mater. Today Commun. 7 (2016) 155–160.
[42] L.A. Franco, A. Sinatora, 3D surface parameters (ISO 25178-2): actual meaning of Spk and its relationship to Vmp, Precis. Eng. 40 (2015) 106–111.
[43] F. Blateyron, The Areal Field Parameters, in Characterisation of Areal Surface Texture, Springer, 2013, pp. 15–43.
[44] A. Larson, R. Von Dreele, Report LAUR 86–748, Los Alamos National Laboratory, New Mexico, USA, 2000.
[45] E. Takahashi, I. Kushiro, Melting of a dry peridotite at high pressures and basalt magma genesis, Am. Mineral. 68 (9–10) (1983) 859–879.
[46] Jun Tong, Han-Xiong Huang, Min Wu, Facile green fabrication of well dispersed poly (vinylidene fluoride)/graphene oxide nanocomposites with improved properties, Compos. Sci. Technol. 129 (2016) 183–190.
[47] A. Cui, et al., Effect of micro-sized SiO 2-particle on the performance of PVDF blend membranes via TIPS, J. Membr. Sci. 360 (1) (2010) 259–264.
[48] J. Chen, et al., Effect of organoclay on morphology and electrical conductivity of PC/PVDF/CNT blend composites, Compos. Sci. Technol. 94 (2014) 30–38.
[49] K.F. Babu, W.M. Choi, Thermal actuation properties of bimorph based on PVDF/rGO composites, Compos. Sci. Technol. 122 (2016) 82–89.
[50] S.J. Oh, N. Kim, Y.T. Lee, Preparation and characterization of PVDF/TiO 2 organic–inorganic composite membranes for fouling resistance improvement, J. Membr. Sci. 345 (1) (2009) 13–20.
[51] Z. Li, et al., Effects of the porous structure on conductivity of nanocomposite polymer electrolyte for lithium ion batteries, J. Membr. Sci. 322 (2) (2008) 416–422.
[52] S. Chen, et al., Self-polarized ferroelectric PVDF homopolymer ultra-thin films derived from Langmuir–Blodgett deposition, Polymer 53 (6) (2012) 1404–1408.
[53] W. Ma, H. Yuan, X. Wang, The effect of chain structures on the crystallization behavior and membrane formation of poly(vinylidene fluoride) copolymers, Membranes 4 (2) (2014) 243–256.
[54] L. Li, et al., Studies on the transformation process of PVDF from α to β phase by stretching, RSC Adv. 4 (8) (2014) 3938–3943.
[55] V. Eswaraiah, V. Sankaranarayanan, S. Ramaprabhu, Inorganic nanotubes reinforced polyvinylidene fluoride composites as low-cost electromagnetic interference shielding materials, Nanoscale Res. Lett. 6 (1) (2011) 137.
[56] F. Ping, et al., Graphene/poly(vinylidene fluoride) composites with high dielectric constant and low percolation threshold, Nanotechnology 23 (36) (2012) 365702.
[57] M. Benz, W.B. Euler, Determination of the crystalline phases of poly (vinylidene fluoride) under different preparation conditions using differential scanning calorimetry and infrared spectroscopy, J. Appl. Polym. Sci. 89 (4) (2003) 1093–1100.
[58] S. Roy, et al., Enhanced electroactive β-phase nucleation and dielectric properties of PVdF-HFP thin films influenced by montmorillonite and Ni (OH) 2 nanoparticle modified montmorillonite, RSC Adv. 6 (26) (2016) 21881–21894.